MATEC Web of Conferences **33**, 05004 (2015)
DOI: 10.1051/matecconf/20153305004

First-principles and Monte Carlo studies of C-doped $Ni_{45}Co_5Mn_{37}In_{13}$ Heusler alloys

Vladimir Sokolovskiy[1a], Vasiliy Buchelnikov[1], and Peter Entel[2]

[1]*Chelyabinsk State University, Condensed Matter Department, 454001 Chelyabinsk, Russia*
[2]*University of Duisburg-Essen, Faculty of Physics and Center for Nanointegration, CENIDE, D-47048 Duisburg, Germany*

Abstract. In this work, we report the study of the effect of carbon on electronic and magnetic properties of the $Ni_{45}Co_5Mn_{37}In_{13}$ alloy. Two compounds with addition of 5 at.% C for Mn and In with ferro- and ferrimagnetic spin configurations have been discussed in the framework of first-principles and Monte Carlo calculations. In order to calculate the magnetic exchange parameters, magnetic moments, and electronic density of states curves we have used the SPR-KKR package. We have shown that the addition of carbon leads to enhancement of antiferromagnetic exchange interactions between Mn atoms in martensite of both compounds. The temperature dependences of magnetizations as well as Curie temperatures of austenite and martensite have been obtained.

1 Introduction

In recent years, Ni-Mn-Z (Z = *sp* element) alloys have gained increasing interest for their potential application as multifunctional materials because of their diverse properties, which include the ferromagnetic shape memory effect, magnetocaloric effect (MCE), large magneto-resistance and exchange bias effect [1-5]. In general, the physical properties of Heusler alloys with different chemical composition are related to the strong coupling between a complex magnetism and a crystal lattice. Moreover, due to the different atomic configuration the competing ferromagnetic (FM), ferrimagnetic (FIM) and antiferromagnetic (AFM) orders can be expected in the off-stoichiometric alloys because of Rudermann-Kittel-Kasuya-Yoshida (RKKY)-type exchange interactions between Mn atoms [6, 7]. As the result, in the majority of Ni-Mn-Z alloys the high-temperature austenitic phase is FM with a high magnetization while the low-temperature martensitic phase is FIM or AFM with a low magnetization. We note that the largest AFM coupling is found between Mn_Y and Mn_Z atoms located in tetragonal crystal. Here, Mn_Y are Mn atoms occupying a regular Mn sublattice while Mn_Z are excess Mn atoms substituted for Z atoms.

Among extensive researches on ternary and quaternary Ni-Mn-Z and Ni-Y-Mn-Z (Y = 3*d* element), there were few reports on the substitution of C in these alloys [8-10]. The modifying Mn_Y-Mn_Z distance can be expected caused by doping C element. Hence, because of the smaller ionic radius of C, the decrease of the cell volume would result in the decrease of the Mn_Y–Mn_Z distance, and as a consequence, tune both the martensitic transformation temperature (T_m) and the Curie temperatures of austenite (T_C^A) and martensite (T_C^M). The effect of the carbon on the martensitic transformation of Ni-Mn-Ga Heusler alloys has been discussed by Lu *et al.* [8] and Chen *et al.* [9]. In both studies the substitution of 1.6 at.% C for Ga content was found to increase the T_m temperature and to disappear the intermartensitic transformation from five-layer modulated martensite to non-modulated martensite. Recently, Zhang *et al.* [10] studied the MCE and mechanical properties of carbon-doped $Ni_{43}Mn_{46}Sn_{11}C_x$ (x = 0, 2, 4, 8) alloys. They have shown that T_m temperatures increase with carbon increasing. Besides, the largest magnetic entropy change, ΔS_m of 34.6 J/(kgK), has been observed for compound with x = 2 for a field change of 5 T.

In the current study, in order to extend our knowledge as a carbon influence on properties of Ni-Co-Mn-In alloys, we use first-principles and Monte Carlo (MC) calculations to investigate their electronic and magnetic properties in dependence on different substitutions of C for In and Mn_Y atoms.

2 Ab initio details and results

To perform the electronic structure calculations, we have used the spin-polarized relativistic Korringa-Kohn-Rostoker (SPRKKR) band structure code [11] in conjunction to the Perdew-Burke-Ernzerhof (PBE) formulation of the generalized gradient approximation (GGA) to the exchange-correlation potential [12]. The calculation of the magnetic exchange couplings, magnetic moments, and density of states (DOS) curves for C-doped NiCoMnIn alloys have been carried out for the austenitic $L2_1$ structure (space group $Fm\underline{3}m$) and for the martensitic $L1_0$ structure (space group *Fmmm*). We have used the

[a] Corresponding author: vsokolovsky84@mail.ru

Article available at http://www.matec-conferences.org or http://dx.doi.org/10.1051/matecconf/20153305004

lattice constants and tetragonal ratio, c/a, from the energy relaxation calculations performed for supercell approach. We have taken into account two compositions with substitution of 5% C for In and for Mn_Y atoms. For each composition the FM and FIM reference states were considered. In the case of FM state, all spins of Ni, Co Mn_Y and Mn_Z atoms are parallel, while in the case of FIM state, the spin of Mn_Z atom is reversed. The effect of chemical disorder is taken by using the single-site coherent-potential approximation (CPA). The Heisenberg exchange coupling constants were calculated, using the equation proposed by Liechtenstein *et al.* [13]. The maximum number of CPA iterations and the CPA tolerance were set to 20 and 0.01 mRy, respectively. The first step in these calculations is to calculate the self-consistent potential (SCF). For SCF cycles, the scattering path operator was calculated with the special point method using a regular k-mesh grid of 57^3 with 4495 k points. All calculations were converged to 0.01 mRy of the total energy.

To achieve this convergence, we have used the BROYDEN2 scheme [14] with the exchange-correlation potential of PBE. For the SCF calculations the arc-like contour path in the complex energy plane has been chosen as in approach of weakly bound states which are treated as core states. The upper end of the energy path E_{max} is set to the Fermi energy E_F. Regarding the real part of lowest energy value we have used the value of $E_{min} = -0.1$ Ry. The number of E-mesh points was set to 30. In order to achieve faster convergence, the SCF mixing parameter was set to 0.20. The maximum number of SCF iterations was taken to 200. The self-consistent potential, which was calculated for the optimized lattice parameter, is then used to calculate the exchange parameters and DOS. For that we have taken the spin-polarized scalar-relativistic (SP-SREL) Hamiltonian with an orbital momentum cutoff of $l_{max} = 2$ on a grid of 57^3, i.e., 4495 $\boldsymbol{k}$ points. The exchange coupling parameters are calculated with respect to the central site i of a cluster atoms with the radius $R_{clu} = \max|R_i - R_j|$. We have taken the radius of a sphere R_{clu} of 2.0.

For the lattice parameters and c/a ratio we have used the values listed in Table 1.

Table 1. Equilibrium lattice parameter and tetragonal ratio, c/a, for C-doped $Ni_{45}Co_5Mn_{37}In_{13}$ alloys with substitution of 5% of C for In and Mn atoms.

Composition	a_0 (Å)	c/a
$Ni_{45}Co_5Mn_{37}In_{13}$	5.96	1.21
Substitution of C for In	5.845	1.33
Substitution of C for Mn	5.85	1.35

2.1 Magnetic exchange parameters

In this subsection we present results of *ab initio* calculations of magnetic exchange coupling constants of carbon-doped Ni-Co-Mn-In alloys. The Heisenberg exchange parameters were calculated with the SPR-KKR package and lattice parameter a_0 and fixed c/a ratio. Note that the lattice parameters for martensite were taken from the condition considering that a cell volume does not change with tetragonal distortions.

Figures 1 and 2 show the calculated J_{ij} exchange parameters in austenite and martensite of C-doped Ni-Co-Mn-In alloys calculated for different spin configurations. Here, we consider two compositions with the substitution of 5% C for In and for Mn_Y atoms. In order to compare results, we also present here the exchange interactions for the case of $Ni_{45}Co_5Mn_{37}In_{13}$ alloy.

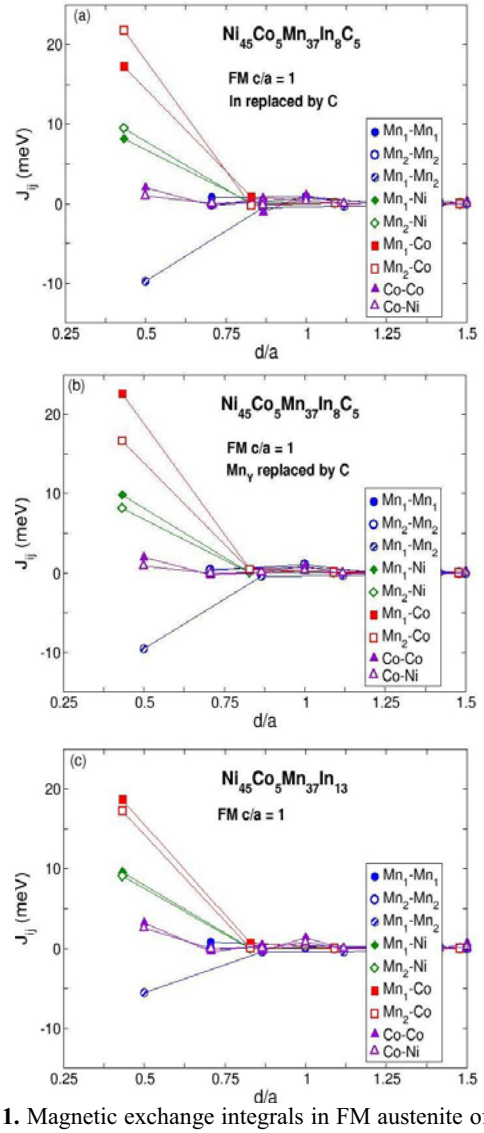

Figure 1. Magnetic exchange integrals in FM austenite of (a, b) C-doped $Ni_{45}Co_5Mn_{37}In_{13}$ and (c) $Ni_{45}Co_5Mn_{37}In_{13}$ alloys as a function of the distance between atoms.

With respect to the J_{ij} interactions of austenite in Fig. 1, we see that the carbon addition increases both, the FM $Mn_{Y(Z)}$-Co interaction and the AFM Mn_Y-Mn_Z interaction between nearest neighbors atoms as well as Mn-Ni interaction does not practically change. Large Mn-Co and Mn-Ni interactions in the first coordination shell are responsible for a high Curie temperature of austenite. Note that these large interactions also due to the short distance between Mn and Co, Ni atoms (in a case that Co substitutes for Ni).

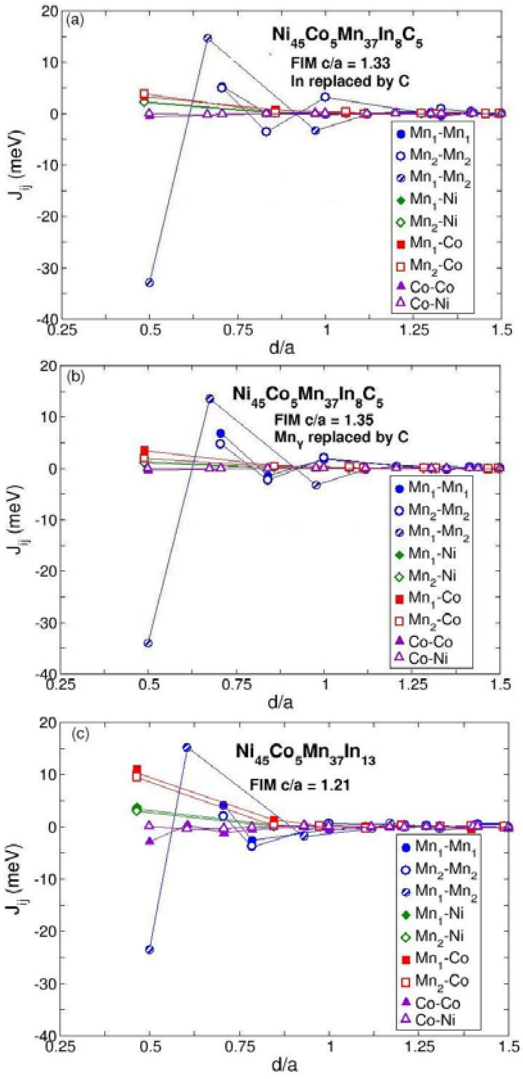

Figure 2. Magnetic exchange integrals in FIM martensite of (a, b) C-doped $Ni_{45}Co_5Mn_{37}In_{13}$ and (c) $Ni_{45}Co_5Mn_{37}In_{13}$ alloys as a function of the distance between atoms.

Regarding the exchange parameters of martensite in C-doped Ni-Co-Mn-In alloys shown in Fig. 2, it is seen that the AFM Mn_Y-Mn_Z interaction increases while the FM Mn-Co and Mn-Ni interactions decreases with carbon addition. Besides, the Mn_Y-Mn_Z interaction shows the most striking oscillatory behavior from AFM to FM interaction. As the result, this interaction in the first coordination shell has a large AFM value of $J_{ij} \approx -35$ meV and then it changes sign and reaches large FM value of $J_{ij} \approx 15$ meV in the next coordination shell. The enhancement of AFM interaction between Mn atoms in martensite can be related with decrease in the lattice parameters a and b leading to a reduction in the Mn_Y-Mn_Z distance. Generally, low values of the Curie temperature of martensite are expected because of weak FM interactions between Mn and Co, Ni atoms and strong AFM interactions between Mn atoms.

2.2 Density of states

The calculated spin-polarized total and partial DOS of FM austenite and of FIM martensite in C-doped Ni-Co-Mn-In alloys are presented in Fig. 3 and 4, respectively. First, let us discuss the DOS curves in FM austenite.

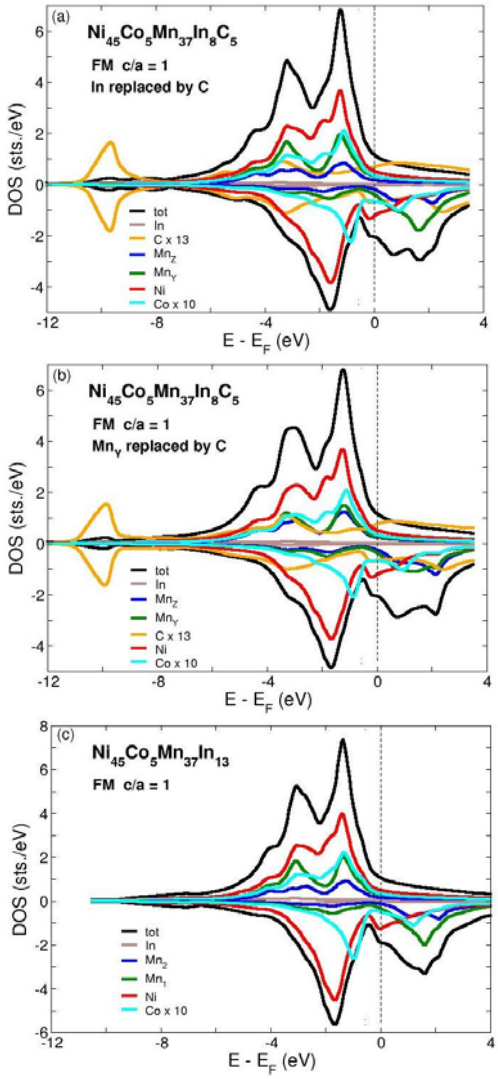

Figure 3. Total and partial DOS curves for FM austenite of (a, b) C-doped $Ni_{45}Co_5Mn_{37}In_{13}$ and (c) $Ni_{45}Co_5Mn_{37}In_{13}$ alloys.

It can be seen from Fig. 3 that the antibonding parts of the DOS around and above the Fermi level E_F have mostly contributions from Mn_Y and Mn_Z 3*d* states, while bonding parts and non-bonding parts have Mn_Y, Mn_Z, and Ni 3*d* contributions. Besides, the small peak at -10 eV on the total DOS is related with the contribution of the *s* electronic states of carbon. In general, for spin-up electronic states two main peaks below the E_F in the Mn_Y and Mn_Z 3*d* states coincide with peaks of the Ni 3*d* states, resulting the strong coupling between atoms.

Regarding the DOS curves for martensite of C-doped Ni-Mn-In alloys, we can see from Fig. 4 that it consists also of the lower part containing mainly *s*-states of carbon at -10 eV and the higher bonding and antibonding parts. The antibonding parts of the DOS around and above the E_F have dominantly 3*d*-states of Mn_Y, Mn_Z atoms, while bonding parts have Mn_Y and Ni 3*d* contributions. The difference of contributions to bonding and non-bonding parts for austenite and martensite is associated with the reversed magnetic moment of Mn_Z in martensite compared to their parallel magnetic moment in

austenite. Additionally, for spin-up anti-bonding states the small peak observed above E_F is caused by contributions from Mn_Z 3*d* bands. It is also found that the contributions from Mn_Y and Mn_Z 3*d* bands to the total DOS are opposite to each other. For the majority DOS of Mn_Y, the main two peaks below E_F are occupied while for the minority DOS, the antibonding peak is above E_F. As the result, the total magnetic moment is found to reduce. We can also observe for austenite and martensite of the $Ni_{45}Co_5Mn_{37}In_8C_5$ alloy with substitution of 5% of C for Mn_Y (Figs. 3(b) and 4(b)), that the partial DOS curves for both Mn_Y and Mn_Z atoms are similar because of close concentrations of Mn_Y and Mn_Z atoms in this compound. With respect to the 3*d* bands of Ni for both, austenite and martensite (Figs. 3 and 4), majority and minority spin states are practically symmetrical, which results in the small magnetic moment of Ni. Since the concentration of C and Co atoms is small, they contribute little to the total DOS. Finally, the pseudogap at the Fermi level is found from Fig. 4 providing the stabilization of the martensitic phase.

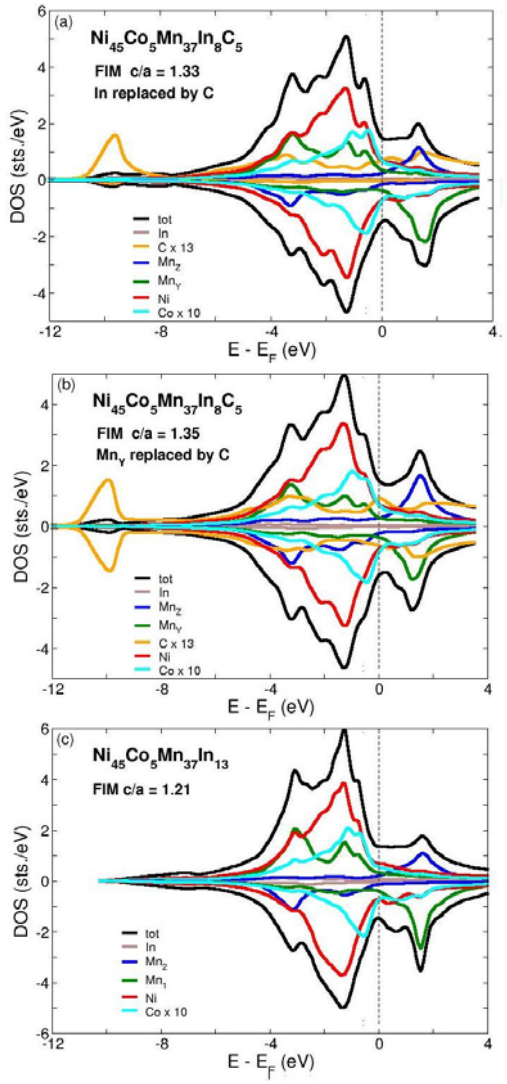

Figure 4. Total and partial DOS curves for FIM martensite of (a, b) C-doped $Ni_{45}Co_5Mn_{37}In_{13}$ and (c) $Ni_{45}Co_5Mn_{37}In_{13}$ alloys.

3 Monte Carlo details and results

3.1. *q*-state Potts Hamiltonian

The magnetic exchange parameters in a combination with partial magnetic moments can be used to simulate a temperature behavior of magnetization and determine T_C^A and T_C^M temperatures by means of MC method. In MC simulations, we use the real lattice with periodic boundary conditions. The unit cell of Heusler alloys is comprised of four interpenetrating *fcc* sublattices with In at site (0, 0, 0), Mn at (1/2, 1/2, 1/2) and Ni at sites (1/4, 1/4, 1/4) and (3/4, 3/4, 3/4), respectively. For the construction of C-doped $Ni_{45}Co_5Mn_{37}In_{13}$ alloys, the configurations of Co, Mn_Z and C atoms on the Ni, In, and Mn_Y sublattices, respectively, take randomly and their total number are fixed by nominal composition.

In this study we use the *q*-state Potts Hamiltonian, which allows us to simulate the first and second order magnetic phase transitions [15]. Here, *q* is the number of possible spin states, $2S + 1$. Since magnetic moments of C and In atoms are negligible, we consider only three types of magnetic atoms in C-doped Ni-Co-Mn-In. As the result, we use the mixed 3-4-6 Potts model. Where, 3, 4, and 6 correspond to the maximum possible spin states for Ni, Co, and Mn [14]. The magnetic Hamiltonian without external magnetic field may be written as

$$H_{mag} = -\sum_{<i,j>} J_{ij}\delta_{S_i,S_j}. \qquad (1)$$

Here, J_{ij} are the exchange parameters obtained from *ab initio* calculations, which may become FM ($J_{ij} > 0$) or AFM ($J_{ij} < 0$). S_i is a spin defined on the lattice site $i = 1...N$. The Kronecker symbol, $\delta_{Si,Sj}$, restricts spin-spin interactions to the interactions between the same $q(Mn_{Y(Z)})$, q(Co), and q(Ni) states. The summation is taken over neighbor pairs up to the six coordination shells.

The magnetization of the 3-4-6 state Potts model is defined in the following way:

$$m_n = \frac{1}{N_n}\left(\frac{q_n N_n^{\max} - N_n}{q_n - 1}\right), \qquad (2)$$

where, *n* denotes a magnetic atom type (Ni, Co, Mn_Y, or Mn_Z), N_n is the total number of type of atom *n*, q_n is the number of magnetic states of atom type *n*, and $N_n^{\max}$ is the maximum number of identical magnetic states on the lattice of type of atom *n*.The total magnetization C-doped $Ni_{45}Co_5Mn_{37}In_{13}$ alloys can be written as

$$M = \mu_{Ni}m_{Ni}(1-x) + \mu_{Co}m_{Co}x + \mu_{Mn_Y}m_{Mn_Y} + \mu_{Mn_Z}m_{Mn_Z}y. \qquad (3)$$

Here, x and y are the concentrations of Co and Mn_Z atoms, respectively. μ_n are the magnetic moments of Ni, Co, Mn_Y, and Mn_Z atoms calculated from *ab initio* simulations and listed in Table 2.

Table 2. Total and partial magnetic moments (in μ_B) in the austenite and martensite of C-doped $Ni_{45}Co_5Mn_{37}In_{13}$ alloys with substitution of 5% of C for In and Mn atoms.

Composition	μ_{MnY}	μ_{MnZ}	μ_{Ni}	μ_{Co}	μ_{tot}
C for In (c/a = 1)	3.54	3.53	0.52	1.31	6.39
C for In (c/a = 1.33)	3.44	-3.43	0.17	0.40	2.14
C for Mn_Y (c/a = 1)	3.43	3.64	0.54	1.33	6.40
C for Mn_Z (c/a = 1.35)	3.28	-3.57	0.09	0.34	0.43
C = 0 at.% (c/a = 1)	3.62	3.76	0.52	1.31	6.63
C = 0 at.% (c/a = 1.35)	3.57	-3.85	0.19	0.73	2.20

3.2 Model results

In this section we present results of modelling a temperature behavior of magnetization curves for austenite and martensite of C-doped $Ni_{45}Co_5Mn_{37}In_{13}$ alloys. The MC calculations carried out by means of the classical Metropolis algorithm. Change in the independent variables q(Ni), q(Co) and $q(Mn_{Y(Z)})$ are accepted or rejected according to a single-site transition probability $W = \{1, \exp(-\Delta H_{mag}/k_BT)\}$, where k_B is the Boltzmann constant. The number of sites used in the simulation is 3925. Thus, in the stoichiometric case, Ni_2MnIn, we have a lattice containing 1098 Mn_Y, 1728 Ni, and 1099 In atoms. As noted above, for off-stoichiometric compositions, the random distribution of Mn_Z, Co, and C atoms at the In, Ni, and Mn_Y sublattices was proposed. As time unit, we used one MC step consisting of N attempts to change the q variables. For a given temperature, the number of MC steps at each site was 5×10^5. The simulations started from the FM austenite and FIM martensite. The system energy H_{mag} and the order parameter m (magnetization) were averaged over 1225 configurations for each of the 400 MC steps. In order to obtain equilibrium values of H_{mag} and m, the first 10^4 MC steps were discarded. The magnitudes of spin states (i.e. q variables) were taken to correspond to a random number r, $0 \le r \le 1$, according to the scheme: if $0 \le r \le l/3$, consequently q(Ni) = l, l = 1, 2, 3, if $0 \le r \le k/4$, consequently q(Co) = k, k = 1 . . . 4, finally, if $0 \le r \le t/6$, consequently $q(Mn_{Y(Z)}) = t$, t = 1 . . . 6.

The temperature behaviors of magnetization curves for austenite and martensite of C-doped $Ni_{45}Co_5Mn_{37}In_{13}$ alloys are shown in Fig. 5. We ca see that the addition of carbon results in decrease in the Curie temperatures of austenite and martensite as compared with the $Ni_{45}Co_5Mn_{37}In_{13}$ alloy. In the cases of compounds with substitution of C for In and Mn_Y atoms, we can see that the T_C^M temperatures are similar ($T_C^M \approx 210$ K), whereas the T_C^A temperatures are slightly different. For instance, the compound with substitution 5 %at. of C for Mn_Y have T_C^A about of 350 K while for other alloy, it is closed to 320 K. In general, the decrease in Curie temperatures with carbon addition is related to enhancement of AFM interactions between Mn and to reduction of FM Mn-Ni and Mn-Co interactions.

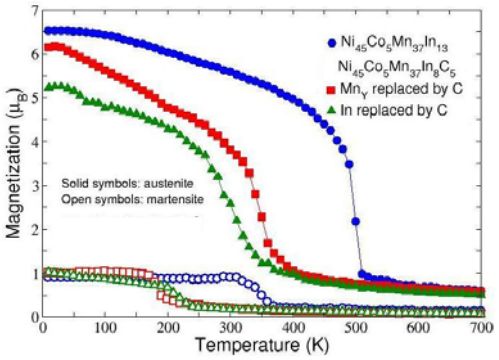

Figure 5. Magnetization curves for austenite and martensite of C-doped $Ni_{45}Co_5Mn_{37}In_{13}$ as a function of temperature. Here, curves with solid (open) symbols correspond to results for austenite (martensite), respectively.

4 Conclusions

In this study, we combined the *ab initio* and Monte Carlo calculations to investigate the magnetic and electronic properties of carbon-doped $Ni_{45}Co_5Mn_{37}In_{13}$ Heusler alloys. Two magnetic spin configurations referred as FM and FIM were considered. It was shown that the addition of carbon resulted to an increase in the FM $Mn_{Y(Z)}$-Co interaction and the AFM Mn_Y-Mn_Z interactions between nearest neighbors atoms in austenite. Contrary to that in the case of martensite, it was found an enhancement of AFM interactions between Mn and a reduction of FM Mn-Ni and Mn-Co interactions with carbon doping. As the result, a decrease in the Curie temperatures of austenite and martensite has been observed. However, the large change in a magnetization between austenite and martensite was observed. Therefore, we can assume that carbon-doped Ni-Co-Mn-In Heusler alloys are interesting materials in the field of magnetic cooling technology. The modelling of MCE in such compounds still needs to be considered, but this is beyond the scope of this study.

Acknowledgments

This work is supported by RFBR Grant No. 14-02-01085, RSF No. 14-12-00570\14 (Section 2), Ministry of Education and Science of Russian Federation (RF) No 3.2021.2014/K (Section 3). PE acknowledges DFG (SPP 1599) for financial support.

References

1. A.N. Vasiliev, V.D. Buchelnikov, T. Takagi, V.V. Khovailo and E.I. Estrin, Physics-Uspekhi **46**, 559 (2003)
2. A. Planes, Ll. Manosa, Mater. Sci. Forum **512**, 145 (2006)
3. M. Khan, I. Dubenko, S. Stadler, N. Ali, J. Phys. Condens. Matter **20**, 235204 (2008)
4. A. Planes, Ll. Manosa, M. Acet, J. Phys. Condens. Matter **21**, 233201 (2009)

5. V.D. Buchelnikov, V.V. Sokolovskiy, Phys. Metal. Metallogrh. **112**, 633 (2011)
6. E. Sasioglu, L.M. Sandrantskii, P. Bruno, Phys. Rev. B **70**, 024427 (2004).
7. J. Rusz, L. Bergvist, J. Kudrunovsky et al. Phys. Rev. B 73, 214412 (2006)
8. X. Lu, X. Chen, L. Qin et al., J. Phys. IV France **112**, 917 (2003)
9. X.Q. Chen, X. Lu, Z.X. Qin, Mater. Sci. Tech. **25**, 829 (2009)
10. Y. Zhang, J. Liu, Q. Zheng et al., Scripta Mater. **75**, 26 (2014)
11. H. Ebert, SPR-KKR package Version 6.3 on http://ebert.cup.uni-muenchen.de
12. J.P. Perdew, K. Burke, M. Enzerhof, Phys. Rev. Lett. **77**, 3865 (1996)
13. A.I. Liechtenstein, M.I. Katsnelson, V.A. Gubanov, J. Phys. F: Met. Phys. **14**, L125 (1984)
14. C.G. Broyden, Math. Comp. **19**, 577 (1965)
15. F.Y. Wu, Rev. Mod. Phys. **54**, 235 (1982)